Experimental study of the crystallization of sodium sulfate hydrates through temperature monitoring

M F C Denecker, R L Hebert, J. Wassermann, G. Dosseh, B. Menendez, A. Bourgès

Environ Earth Sci
DOI 10.1007/s12665-014-3379-2

ORIGINAL ARTICLE

Experimental study of the crystallization of sodium sulfate hydrates through temperature monitoring

M. F. C. Denecker · R. L. Hebert · J. Wassermann · G. Dosseh · B. Menendez · A. Bourgès

Received: 19 December 2013 / Accepted: 21 May 2014

Abstract Sodium sulfates are well known to be the most damaging salts in building materials and rocks. Unfortunately, the crystallization processes of sodium sulfates are not completely understood. In addition, the metastable heptahydrate has long been neglected in scientific works on salt damage until recently. In this study, we use temperature monitoring and differential scanning calorimetry to detect and identify the crystallization of sodium sulfate hydrates (i.e., mirabilite and heptahydrate) upon cooling/heating a bulk solution. The presence of impurities seems to play a major role in the crystallization sequence and can explain the crystallization of mirabilite and ice close to −10 °C. The crystallization of heptahydrate does not seem to be sensitive to the presence of impurities and does not always occur prior to the crystallization of mirabilite as commonly observed. The heptahydrate and mirabilite show different and characteristic thermal signatures that enable to distinguish each other. The shape, the intensity and the duration of the peak of temperature due to the crystallization depict these differences. Therefore, the thermal signatures can be used in further experimental studies to estimate the role of the different sodium sulfate hydrates involved in the salt weathering of rocks.

Keywords Sodium sulfates · Heptahydrate · Thermal signature · Temperature monitoring · Impurity

M. F. C. Denecker (✉) · R. L. Hebert · J. Wassermann · B. Menendez
Géosciences et Environnement Cergy, Université de Cergy-Pontoise, 5 mail Gay-Lussac, 95031 Cergy-Pontoise Cedex, France
e-mail: melanie.denecker@u-cergy.fr

G. Dosseh
Laboratoire de Physicochimie des Polymères et des Interfaces, Université de Cergy-Pontoise, 5 mail Gay-Lussac, 95031 Cergy-Pontoise Cedex, France

A. Bourgès
Laboratoire de Recherche des Monuments Historiques, 29 rue de Paris, 77420 Champigny sur Marne, France

Introduction

Sodium sulfates are recognized to be the most damaging salts in historical and modern porous building materials (Rodriguez-Navarro and Doehne 1999; Tsui et al. 2003; Rijniers et al. 2005) as well as in terrestrial and Martian rock weathering processes (Goudie and Viles 1997; Malin 1974). As shown in the Na_2SO_4–H_2O phase diagram (Fig. 1), the sodium sulfates can occur under four different phases under room conditions: (1) Two anhydrous polymorphs (thenardite and unrepresented phase III) and (2) two hydrates (mirabilite and heptahydrate). Thenardite (Thn; also known as form V, Na_2SO_4) and phase III are, respectively, stable and metastable above +32.4 °C. Phase III is frequently observed during the evaporation of a sodium sulfate solution (Amirthalingam et al. 1977; Grossi et al. 1997). Mirabilite (Mir; SS10) is a decahydrate ($Na_2SO_4{\cdot}10H_2O$) that is stable below +32.4 °C, and the heptahydrate (SS7; $Na_2SO_4{\cdot}7H_2O$) is metastable below +23.5 °C (Washburn and Clem 1938) as shown in Fig. 1. These limit temperatures of stability (for SS10) and metastability (for SS7) correspond to peritectic reactions where the hydrates undergo an incongruent melting to form Thn. These temperatures are higher when peritectic reactions produce anhydrous form III (+34.06 °C for mirabilite, +28.25 °C for heptahydrate; Steiger and Asmussen 2008).

Thn and phase III can crystallize directly upon evaporation of a sodium sulfate solution above +32.4 °C

Published online: 07 June 2014

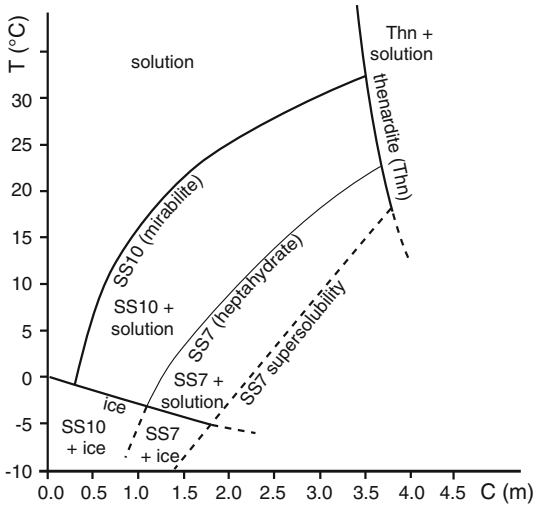

Fig. 1 Na_2SO_4–H_2O phase diagram (after Hartley et al. 1908) at room pressure showing stable (*solid lines*) and metastable (*dashed lines*) phase boundaries. *m* molality

(Amirthalingam et al. 1977; Grossi et al. 1997) and also by dehydration of mirabilite (Rodriguez-Navarro et al. 2000). SS10 and SS7 can crystallize upon evaporation of a sodium sulfate solution below +32.4 °C (Shahidzadeh-Bonn et al. 2008; Saidov 2012), as well as upon cooling of a saturated solution (e.g., Gans 1978; Espinosa-Marzal and Scherer 2008; Derluyn et al. 2011; Saidov et al. 2012). The crystallization of sodium sulfates in bulk solution and the crystallization in limestones were investigated by Espinosa-Marzal and Scherer (2008) through cooling–heating cycles from +50 to −10 °C with a cooling–heating rate of 0.25 °C/min. Differential scanning calorimetry (DSC) was performed in these studies showing that SS10 crystallizes close to or below 0 °C. At a faster cooling rate (10–20 °C/min), the crystallization can occur even at negative temperature. They also observed that SS7 crystallizes prior to SS10.

Though it is known since the 19th century (Loewel 1850), SS7 has been neglected in modern works about salt weathering until recently (Rijniers et al. 2005; Genkinger and Putnis 2007; Espinosa-Marzal and Scherer 2008; Hamilton et al. 2008; Hamilton and Hall 2008; Hall and Hamilton 2008; Oswald et al. 2008; Derluyn et al. 2011; Saidov et al. 2012). Recently, Derluyn et al. (2011) and Saidov (2012) studied the cooling-induced growth of metastable SS7 crystal by combining nuclear magnetic resonance (NMR), concentration measurement of the solution and time-lapse microscopy. Solutions with different concentration were cooled from approximately +33 °C with a cooling rate of 0.13 °C/min. Crystal growth starts once the supersolubility line of SS7 is reached, decreasing the solution concentration, and ceases when the concentration gets to the SS7 solubility line. Despite these numerous studies on sodium sulfate hydrates, the relationship between SS7 and SS10 is neither straightforward nor clearly understood. Several studies showed that SS10 rarely crystallizes directly from a supersaturated sodium sulfate solution, but that the first solid to form when cooling or evaporating such a brine is the metastable SS7 (Loewel 1850; De Coppet 1901; Hartley et al. 1908; Espinosa-Marzal and Scherer 2008; Hamilton and Hall 2008). For this reason, it is likely that SS7 could play a role in the salt weathering of rocks inducing more damages to porous building materials than the direct crystallization of mirabilite (Espinosa-Marzal and Scherer 2008).

The main mechanisms of rock damage during salt weathering are the crystallization pressure against pore walls, which is proportional to the degree of supersaturation, and the volume variation of the salt structure upon wetting/drying cycles (Rodriguez-Navarro and Doehne 1999; Rodriguez-Navarro et al. 2000; Scherer 2004; Steiger 2005a, b). According to Winkler and Singer (1972), the crystallization pressure of thenardite is greater than that of mirabilite for equal supersaturation ratios. Therefore, several authors suggested that thenardite could induce more damages than mirabilite at low relative humidity (Sperling and Cooke 1985; Rodriguez-Navarro and Doehne 1999), particularly in the case of constant capillary rise (Rodriguez-Navarro et al. 2000). Additional experimental studies revealed that mirabilite crystallization alone could generate sufficient stress to damage most of the stones (Flatt 2002) especially during wetting periods (Tsui et al. 2003). The major damage is observed during the formation of hydrates growing at supersaturation against the pore walls (Rodriguez-Navarro et al. 2000; Flatt 2002; Tsui et al. 2003; Scherer 2004; Steiger and Asmussen 2008). The crystallization of SS10 from thenardite involves the dissolution of the anhydrous phase followed by the crystallization of mirabilite from the highly supersaturated solution (Rodriguez-Navarro et al. 2000). The supersaturation ratio induces a high crystallization pressure causing serious damages (Correns 1949). But crystallization pressure remains a matter of debate (Desarnaud 2009).

The crystallization of sodium sulfates remains partially understood, in particular SS7 and its relationships with the other sodium sulfates as well as its role in rock weathering. SS7 thus became recently the focus of several studies mainly dedicated to its identification and characterization using hi-tech and sometimes expensive analytical devices such as NMR (Hamilton et al. 2008; Pel et al. 2010; Derluyn et al. 2011; Pel and Saidov 2013; Saidov et al. 2013), energy dispersive synchrotron X-ray diffraction (Hamilton and Hall 2008; Hamilton et al. 2008), Raman spectroscopy (Hamilton and Menzies 2010) or DSC (Espinosa-Marzal and Scherer 2008) for example.

The crystallization of sodium sulfate hydrates is an exothermic process (Anderson 1984; Bing et al. 2007). This means that crystallization and dissolution of hydrates could be monitored through temperature measurement of a saturated solution undergoing cooling/heating cycles. As they are two hydrates with different composition and different thermodynamic properties, the crystallization/dissolution of SS7 and SS10 should be thermally distinguished. The exothermic crystallization of hydrates can also be record using DSC (e.g., Espinosa-Marzal and Scherer 2008).

In this study, we investigate the crystallization of sodium sulfate hydrates upon cooling/heating a bulk solution using a simple and affordable tool: temperature monitoring. This method could be used in further experimental works about salt weathering of rocks to allow the identification of the sequence of crystallization/dissolution of sodium sulfate phases and then assess the role of the different hydrates in rock damaging. Additional measurement using DSC is performed to support the temperature monitoring approach used in this study.

Materials and methods

Cooling/heating cycles were performed on solutions with a concentration of 30 weight % of Na_2SO_4 (i.e., $C_i \sim 3.017$ mol). The solution was prepared from anhydrous Na_2SO_4 (Natriumsulfat Roth $\geq$99.0 %) dissolved in demineralized water at +60 °C using a magnetic stirrer to enhance the complete dissolution of salt crystals. The concentration of 30 wt% of Na_2SO_4 was chosen close to the supersaturation condition and also because it is in the same range of concentration used in previous works (Hamilton et al. 2008; Espinosa-Marzal and Scherer 2008; Derluyn et al. 2011; Saidov et al. 2012).

The two methods used in this study consist in (1) temperature monitoring and (2) DSC to identify the thermal signature of the crystallization of the different sodium sulfate hydrates. Thanks to heat flow measurement, DSC can also provide information regarding the nucleation and the crystal growth (Espinosa-Marzal and Scherer 2008). For both studies, the sample holders were first cleaned with demineralized water and secondly dried either with compressed air or by evaporation (at +60 °C in the case of temperature monitoring, and room T for DSC).

Temperature monitoring

In the case of the temperature monitoring, samples of ±2 ml (i.e., 2–2.5 g) of solution were confined in an approximately 25-ml sealed bottle. Samples were placed within a climatic chamber (Binder MKF); a computing program controlled the sequence of cooling/heating cycle (Fig. 2). The cooling/heating cycle used in this study is based and modified from previous works that were proven to be efficient to crystallize SS7 (Derluyn et al. 2011; Saidov 2012) and SS10 (Espinosa et al. 2008). It starts from +50 °C with a cooling phase down to +5 °C where the temperature, close to the SS7 supersolubility line, is hold for 2 h. This first phase aims to crystallize SS7. A second cooling phase, down to −10 °C, takes place to crystallize SS10. At this temperature in the Na_2SO_4–H_2O system, ice is also likely to crystallize, which is an exothermic reaction too. The temperature of −10 °C is hold for 2 h before heating back to +50 °C. Samples remain 3 h at +50 °C to favor the complete dissolution of crystallized salts before the start of a new cycle. A rate of 0.25 °C/min is used for cooling and heating as in Espinosa-Marzal and Scherer (2008). The temperature of the samples was measured with a precision of ±0.1 °C, via a type-K thermocouple dipping in the bottom of the solution (Fig. 2), and recorded every second using a data logger (Agilent).

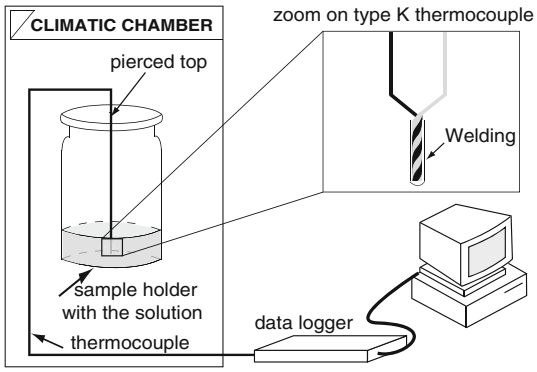

Fig. 2 Experimental set-up for the temperature monitoring; samples are placed in a climatic chamber where they undergo cooling–heating cycles. The temperature is recorded via a type-K thermocouple that dips into the solution at the bottom of the bottle

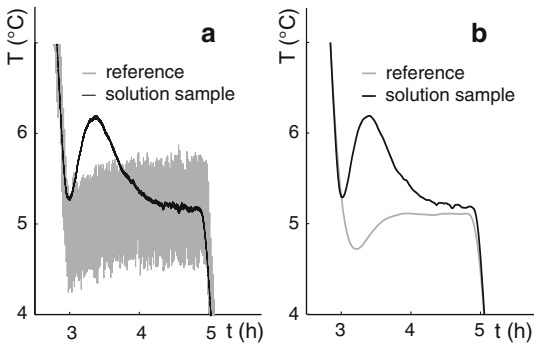

Fig. 3 Signal treatment. T vs. t data for the reference and the solution **a** raw data, **b** after filtering

Basic analysis of the temperature signal

The temperature signal measured in the climatic chamber is used as reference. Raw data appear rather noisy (Fig. 3a) very likely due to the periodic activity of the climatic chamber ventilator.

To separate the temperature signal—resulting from crystal precipitation/dissolution processes—from climatic chamber noise, a frequency filtering was performed. The frequency spectrum of the noisy signal (raw data) is classically obtained using a Fast Fourier Transform. The spectrum analysis allows the identification of the noise characteristic frequencies: from 0.00065 to 0.05 Hz. Then, a low-pass frequency filter was applied. In time domain, the filtered signal provides a smoother shape of the thermal signature by removing the short-term fluctuation and leaving the long-term trend (Fig. 3b).

Differential scanning calorimetry (DSC)

The differential scanning calorimeter Q100 by TA instruments was used to measure the heat flow and the temperature during the crystallization/dissolution processes. The measuring system consists of two identical aluminum pans (an empty pan for the reference sample and another pan for the solution sample), which are hermetically sealed and placed on small platforms within the DSC chamber. A thermocouple sensor is placed below each pan allowing the measurement of temperature, and the calculation of the heat flow. A solution mass (15–30 mg) was used for the analysis of the crystallization/dissolution processes occurring in the solution. The same sequence of cooling/heating cycle as for temperature monitoring was performed, except that the duration of the different plateaus (+50, +5 and −10 °C) has been shortened. This cycle enables a comparison between temperature monitoring results and DSC. The DSC provides the differential heat flow (heat/time) between the sample and the empty reference pan as a function of the sample temperature.

The enthalpy of crystallization

The heat released during the crystallization of salt (Q_c) is linked to the crystallization rate (dn_c/dt). It is written in the following form:

$$Q_c = \Delta H_c \frac{dn_c}{dt}, \tag{1}$$

where ΔH_c is the enthalpy of crystallization of the precipitated salt (J/mol), n_c is the amount of crystallized salt (mol) and t the time. The amount of precipitated salt can be calculated as a function of time and is given by the integration of Eq. (1). To integrate this equation, the crystallization enthalpy must be known as a function of temperature and concentration. But these two parameters change during the phase transition. More studies dealing with heat of crystallization are available in Marliacy et al. (2000) and Espinosa-Marzal and Scherer (2008). To compute the crystallization rate, Eq. (1) must be integrated to get the time-dependant amount of crystallized salt $n_c(t)$:

$$\int Q_c dt = \int \Delta H_c \frac{dn_c}{dt} dt. \tag{2}$$

The amount of crystallized salt Δn_c (mol) is given as a function of an initial concentration (C_i, mol/kg) and a final concentration (C_f, mol/kg) of the solution. It is written in the following form:

$$\Delta n_c = \frac{m_w(C_i - C_f)}{1 - C_f M_w \upsilon}, \tag{3}$$

with m_w, the initial mass of water (kg), M_w the molar mass of water (0.018 kg/mol) and υ the number of mole water necessary for a mole of hydrated salt.

From Eqs. (2) and (3), the average crystallization enthalpy during phase change ΔH_m (J/mol) is given by the following equation:

$$\Delta H_m = \frac{\int Q_c dt}{\Delta n_c}. \tag{4}$$

The variation of the heat flow results from crystallization/dissolution processes. It can be estimated from Eq. (4) and compared with data published by Espinosa-Marzal and Scherer (2008). The variation of the heat flow appears as peak in a heat flow vs time diagram. The shape, the intensity and the duration of the peak can be compared with those observed during temperature monitoring. Indeed, even if they do not show exactly the same parameters, (ΔT in °C for temperature monitoring and heat flow in mW for DSC), those peaks describe the same phenomena (heat released or consumed during phase transition).

Results

In this section, we present the results of the temperature recording during the cooling/heating cycles of a bulk solution also called temperature signal, and of the DSC performed on a bulk solution as well.

Temperature monitoring

8 experiments of temperature monitoring upon cooling/heating cycles were performed on a sodium sulfate solution. Two types of results are observed and are summarized through case 1 (Fig. 4) and case 2 (Fig. 5). Both figures

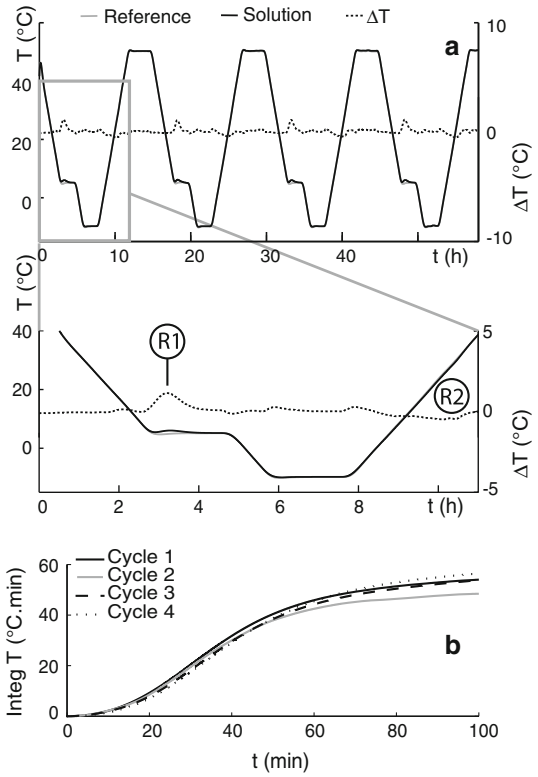

Fig. 4 Temperature monitoring results of case 1. **a** Temperature vs. time diagram of the reference (*gray*) and the solution (*black*) during 4 cooling–heating cycles. ΔT (*dashed line*): difference of temperature between the solution and the reference; *R1* reaction 1; *R2* reaction 2; **b** integral of temperature vs. time for the reaction 1 during each cooling period (cycle 1 to cycle 4)

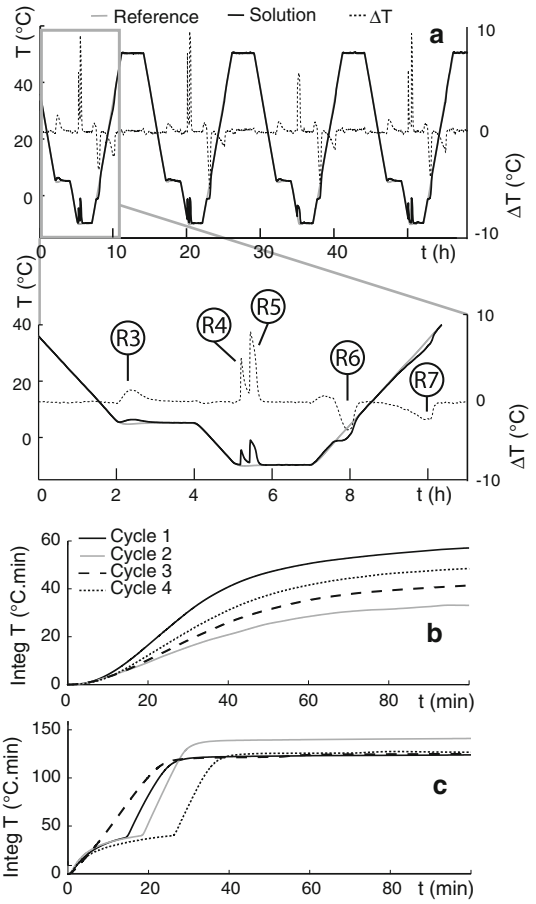

Fig. 5 Temperature monitoring results of case 2. **a** Temperature vs. time diagram of the reference, the solution and ΔT; *R3–R7*: reaction 3–7; **b** integral of temperature vs. time for reaction 3; **c** integral of temperature vs. time for reactions 4 and 5

show, as a function of time, the temperature signal of the climatic chamber (i.e., temperature reference) and the solution sample, as well as ΔT, which is the difference of temperature between the solution and the reference. A positive ΔT indicates a heat production, whilst a negative ΔT indicates a heat consumption, which are linked, respectively to phase crystallization and dissolution.

The first striking feature is that the temperature signal of the bulk solution shows a good reproducibility from a cycle to another for both results.

Figure 4 is a representative example of the results obtained for four experiments. The temperature of the solution follows that of the reference during cooling from +50 °C to the plateau at +5 °C where an exothermic peak (reaction 1) is observed. It forms a smooth asymmetrical peak starting actually at 6.9 ± 0.2 °C. Looking at the ΔT curve, this peak occurs over a large period of time (99 ± 5.7 min), has a low height (peak maximum 1.1 ± 0.1 °C) characterized by a progressive and slow temperature increase. Once the exothermic reaction is over, the temperature of the solution and the reference are identical during cooling from +5 to −10 °C (i.e., ΔT is equal or close to 0 °C). During the heating back to +50 °C we observe a negative variation of the ΔT curve, which indicates an endothermic reaction "2". It starts at 10.3 ± 0.5 °C and finishes at 28.5 ± 0.3 °C, with an inflection point at 22.9 ± 1.8 °C. Above 28.5 ± 0.3 °C, the two temperature curves are indistinguishable until the end of the cycle. Additional minor variations of ΔT are also observed (Fig. 4a) at the changes of temperature orders (i.e, at +5, −10 and +50 °C plateaus). They are characterized by a low peak height of ±0.1 °C which is in the order of magnitude of the temperature measurement accuracy, and they likely result from an inertia problem of the climatic chamber.

Figure 4b shows the temperature integral for each peak linked to the reaction 1 as a function of time. Each integral corresponds to the area below the temperature peak. The integral curves are very similar from a cycle to another, describing a sigmoidal shape and an area around 53.2 ± 2.9 °C min. The homogeneity of the integral curves shows more convincingly the good reproducibility of the results.

Figure 5 is a representative example of the results obtained for the other four experiments. The temperature

Table 1 Peak characteristics of the different observed reactions

Reaction	1	2	3	4	5	6	7
Type of reaction	Exothermic = crystallization	Endothermic = dissolution	Exothermic = crystallization	Exothermic = crystallization	Exothermic = crystallization	Endothermic = dissolution	Endothermic = dissolution
Temperature of appearance (°C)	+6.9 ± 0.2	+10.3 ± 0.5	+5.6 ± 0.1	−8.8 ± 0.8	−9.4 ± 0.4	−1.3 ± 0.1	+18.8 ± 0.8
End of dissolution (°C)	–	28.5 ± 0.3	–	–	–	7.8 ± 0.2	+38.2 ± 0.4
Peak height (°C)	1.08 ± 0.05	–	1 ± 0.3	5.98 ± 1	8.5 ± 0.5	–	–
Peak area (°C min)	49–56	–	33–56	40	80–100	–	–
Inflection point dissolution (°C)	–	+22.9 ± 1.8	–	–	–	−0.1 ± 0.1	+33.2 ± 0.2
Duration (min)	99 ± 5.7	73.3 ± 2.5	78 ± 6.9	16.3 ± 2.1	22.3 ± 2.1	37.5 ± 0.4	59 ± 1.5

signal of the reference is the same as in Fig. 4. This is not the case for the temperature signal of the solution, which shows this time several peaks of temperature. A smooth asymmetrical exothermic peak (reaction 1) is observed at the +5 °C plateau and starts at 5.6 ± 0.1 °C. This exothermic reaction 1 looks like the reaction 1 observed in Fig. 4 (Table 1). After or during cooling to −10 °C, two new exothermic reactions occur corresponding, respectively, to reactions 1 and 5 (Table 1). The reaction 1, which starts at −10 °C during the first cycle, and around −8.8 °C ± 0.8 from cycle 2, shows a narrow peak (duration 16.3 ± 2.1 min) with a brutal increase of temperature and a high peak height. The reaction 5 looks rather similar. Its peak is also narrow but a little bit less (duration 22.3 ± 2.1 min), has a higher height and shows an instantaneous increase of temperature. It is worth noticing that those two peaks can occur separately in time (cycles 1, 2 and 4) or more or less simultaneously (cycle 3).

During the heating stage, a plateau of temperature at ∼ −1.3 ± 0.1 °C, that lasts few minutes, shows an endothermic reaction (reaction 6, Table 1). Once this reaction is completed, the temperature increases to reach the reference curve. A second endothermic reaction (reaction 7) occurs in the temperature range from 18.8 ± 0.8 to 38.2 ± 0.4 °C with a maximum inflection point at 33.2 ± 0.2 °C. Again, once the reaction 7 is over, the temperature profile of the solution fits with the reference.

ΔT (Fig. 5a) shows the different processes of crystallization and dissolution that occur during the cycles and also the difference of heat production according to the phase that is involved. Thus, the crystallization linked to reaction 3 produces less heat than reaction 4 that produces less heat than reaction 5 for a given time. Similarly, we can observe that reactions 4 and 5 are characterized by a high heating rate compared to reaction 3 (respectively, 0.37 ± 0.03, 0.38 ± 0.04 and 0.01 ± 0.01 °C/min). The temperature peak integral of reaction 3 (Fig. 5b) shows more disparity than in the previous experiment (Fig. 4b). Peak area varies in the range 33–57 °C min whilst previously it was in the range 49–56 °C min. Despite the disparity, it is worth noticing that the shape of the curves keeps a certain consistency. Figure 5c shows the evolution of the temperature integral peak for reactions 4 and 5. For cycles 1, 2 and 4, we can observe two steps of evolution: (1) a normal yield curve up to ∼39 °C min and (2) a rapid and linear increase up to a plateau in the range 125–140 °C min. In the case of cycle 3, we do not observe these two steps of evolution but just a linear and progressive increase of the peak area up to ±125 °C min. This can be due to the more or less simultaneous occurrence of the reactions 4 and 5. Note that in all cases, the duration of the crystallization phenomena is between 27 and 41 min, whilst it lasts around 70–87 min in the case of reaction 3 (Table 1).

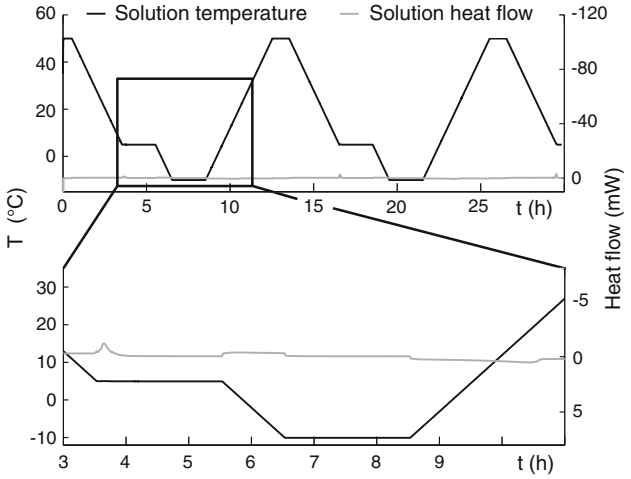

Fig. 6 DSC results of case 1: heat flow and temperature vs. time during 2.5 successive cooling/heating cycles, and zoom on the cycle 1 (sample mass = 27.06 mg)

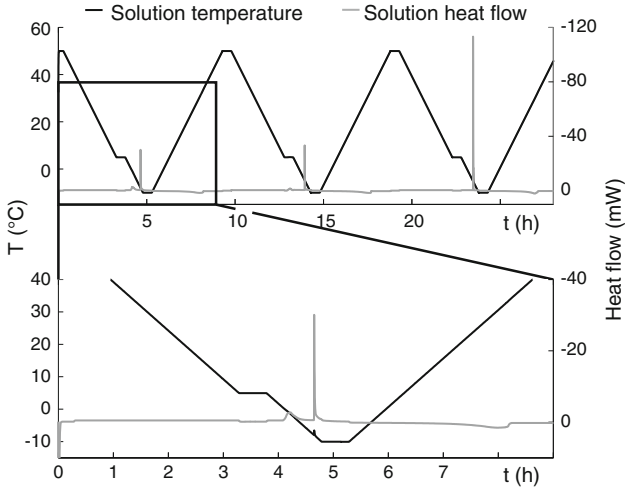

Fig. 7 DSC results of case 2: heat flow and temperature vs. time during 3 successive cooling/heating cycles, and zoom on the cycle 1 (sample mass = 16.98 mg)

Differential scanning calorimetry

Six experiments of DSC upon 2.5 or 3 cooling/heating cycles were performed on a sodium sulfate solution. They show, as for temperature monitoring, two types of results that are summarized in Figs. 6 and 7. Both figures show the temperature and the heat flow vs time of the solution sealed in an aluminum pan.

Figure 6 shows the results obtained for three DSC. The temperature signal of the solution does not present perceptibly any variation during all the experiment. However, the heat flow reveals a small heat production close to the plateau at +5 °C at each cooling cycle. The exothermic reaction occurs as a small and broad peak with a low height. It starts around 5.2 °C and occurs on a time interval equal to 15 min. The characteristics of this exothermic reaction remind those of the peak observed for the reaction 1 during temperature monitoring. During the heating stage of the cycle, we can observe an endothermic reaction between 9.8 and 21.2 °C which can be compared with reaction 2 of the temperature monitoring experiment. The second and the third cycle is a repetition of the first one with the exception of a higher intensity for the peak of heat production.

Figure 7 is a representative example of the results obtained for three other DSC. The heat flow of the solution shows two exothermic peaks during the cooling from +5 to −10 °C for the first cycle. We observe first, a small and smooth exothermic reaction that occurs between 0.5 and −4 °C and lasts around 25 min. The shape and the intensity of the peak suggest that this exothermic reaction is comparable to the reaction 1 even if the temperature of appearance is lower than previously observed (Figs. 4, 5, 6). Secondly, a sharp and intense peak of heat flow matching is observed at around −8 °C. According to the shape and intensity, as well as the temperature of occurrence, this peak could correspond to the reaction 4 observed during the temperature monitoring (Fig. 5). Third, an endothermic and low intensity heat flow peak is observed during the heating stage. This endothermic reaction, that takes place at +17.5 °C and finishes at ∼ +34.0 °C over a large period of time (∼60 min), is very similar to the reaction 7 (i.e., the same temperature range, Table 1).

The second cycle shows similar results with minor exceptions: the first exothermic peak seems to be lower and appears on the plateau at +5 °C. The second exothermic peak is slightly more intense and shifted toward higher temperature that means that the reaction takes place earlier during the cooling stage. The heat flow associated with the endothermic reaction seems to remain the same.

An additional third cycle has been performed. The first small exothermic peak is not observed. On the other hand, the heat flow associated with the second one shows an important increase, the shape of the peak remaining unchanged. The heat flow associated with the endothermic reaction is also more important.

Discussion

Temperature monitoring and DSC were used to study the thermal signature associated with the SS7 and SS10 crystallization, when a sodium sulfate solution is cooled down from +50 to −10 °C. Both experiments show two sets of results. On one hand (case 1), we observe 1 exothermic and 1 endothermic reactions (Figs. 4, 6), and on the other hand (case 2), 2 or 3 exothermic reactions are observed, followed by 1 or 2 endothermic reactions (Figs. 5, 7). To

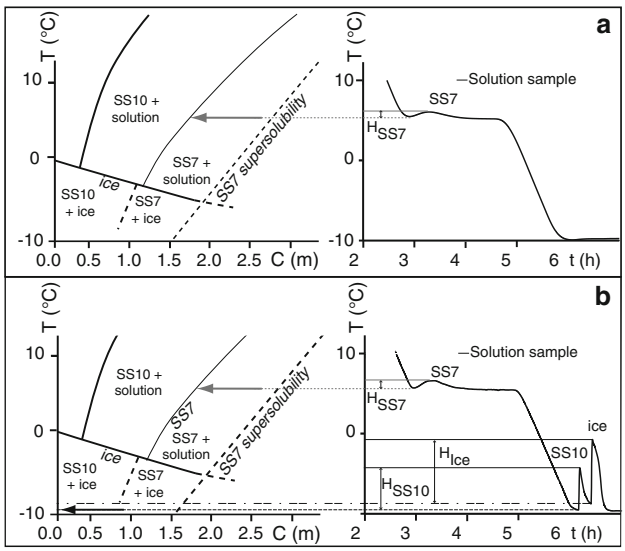

Fig. 8 The thermal signature of each sodium sulfate hydrates and ice with respect to the Na_2SO_4–H_2O phase diagram: **a** Case 1 where only SS7 crystallizes, **b** case 2 where SS7, SS10 and ice crystallize. *H* peak height

analyze our results, we have decided to take into account recent and older studies (Hartley et al. 1908; Washburn and Clem 1938; Hamilton and Hall 2008; Espinosa-Marzal and Scherer 2008; Derluyn et al. 2011; Saidov et al. 2012; Saidov 2012).

In the case 1, both DSC and temperature monitoring show a similar peak due to heat release (reaction 1) during each cooling period precisely at 5.2 and 7.4 °C, respectively. According to Derluyn et al. (2011) and Saidov (2012), this peak corresponds to the crystallization of SS7 once its supersolubility line is reached or crossed (Fig. 8). The temperature signal of the solution shows a good reproducibility from a cycle to another suggesting that the system is reset at the end of each cycle (i.e., that all the precipitated salt crystals are dissolved during the heating at +50 °C). The heat flow obtained by DSC (Fig. 6) shows a lower exothermic reaction in cycle 1 compared to cycles 2 and 3, suggesting that there was less salt to crystallize maybe because the crystallization was more difficult to initiate during the first cooling period.

The amount of SS7 that can precipitate can be calculated from DSC results according to Espinosa-Marzal and Scherer (2008), using Eq. (3). It is $\Delta n_c = 2.05 \times 10^{-5}$ mol at +5 °C (with $C_i = 3.017$ mol/kg and $C_f = 1.65$ mol/kg; C_f, the saturation molality with respect to heptahydrate at this temperature is estimated from the Na_2SO_4–H_2O phase diagram, Fig. 1). The heat measured (Q_{meas}) from the peak in Fig. 6 is 0.534 J for the first cycle, and 0.711 J for the second one. Using Eq. (4), the average enthalpy of crystallization (ΔH_m) for SS7 can be estimated at −26.049 kJ/mol for cycle 1 and −34.683 kJ/mol for cycle 2. If the exothermic reaction observed, for example in cycle 1, was due to the crystallization of SS10, the same calculation would lead to a $\Delta n_c = 3.30 \times 10^{-5}$ mol at +5 °C (with a $C_f = 0.48$ mol/kg with respect to mirabilite) and then a $\Delta H_m = -16.182$ kJ/mol. As the enthalpy of SS10 crystallization is around −62 kJ/mol according to Fig. 3 of Espinosa-Marzal and Scherer (2008), the exothermic reaction observed in case 1 (Fig. 6) can only correspond to the crystallization of SS7. In addition, the calculated ΔH_c in this study (−26.049 and −34.683 kJ/mol at +5 °C) are comparable to the estimation made by Espinosa-Marzal and Scherer (2008). The difference of height between the two heat flow peaks, as well as the difference between the two calculated ΔH_c suggests that there is less SS7 to crystallize during cycle 1.

The endothermic reaction that is observed during temperature monitoring (reaction 1) and DSC experiments corresponds to the dissolution of SS7 that crystallized during the cooling stage. It is comprised between +10 and +28 °C. In this range of temperature we can observe an inflection point corresponding to the disappearance of the last crystal at around +22 ± 1 °C which is close to the upper limit of temperature of SS7's metastability (Washburn and Clem 1938).

In the case 2, both experiments present other sequences of exo- and endothermic reactions. For temperature monitoring (Fig. 5), the reaction 3 is attributed to the crystallization of SS7 because it looks like reaction 1 (Fig. 4a). After cooling until −10 °C, reactions 4 and 5 occur. According to the theoretical cooling of a saturated solution of sodium sulfate within the Na_2SO_4–H_2O system, the peak of reaction 4 corresponds to the crystallization of SS10. The morphology of this peak is consistent with the description made by Espinosa-Marzal and Scherer (2008) for the crystallization of SS10. The peak of reaction 5 corresponds to the formation of ice, which is the third and only last possible solid phase to crystallize within the Na_2SO_4–H_2O system at this temperature. Besides, this reaction has also been observed when performing the same experiment on demineralized water sample. As in case 1, the temperature monitoring of the brine solution presents a good reproducibility from a cycle to another, except for cycle 3 where SS10 and ice crystallize together suggesting that the crystallization occurs at the eutectic condition. In addition, the DSC results show a crystallization peak similar to the reaction 3 but at a lower temperature. It corresponds to the crystallization of SS7 during the first cycle. The shift of SS7 crystallization at lower temperature can be due to an undercooling effect. The second peak at around −8 °C is similar to the reaction 4 and corresponds to the crystallization of SS10.

From DSC data, the amount of SS7 than can crystallize is $\Delta n_c = 4.20 \times 10^{-5}$ mol at −3 °C (with $C_i = 3.017$ and

$C_f = 1.111$ mol/kg) during cycle 1. The heat from the peak is 1.25 J that could lead to a $\Delta H_m = -29.762$ kJ/mol which is once again similar to the published data of Espinosa-Marzal and Scherer (2008). For the second peak at −8 °C, if SS10 crystallizes directly from the cooling of the solution (i.e., SS7 dissolves completely before SS10 crystallization) the amount that can crystallize is $\Delta n_c = 5.44 \times 10^{-5}$ mol at −8 °C (with $C_i = 3.017$ and $C_f = 0.3$ mol/kg; C_f is the concentration value at the eutectic condition) and ΔH_m is calculated equal to −19.610 kJ/mol ($Q_{meas} = 1.067$ J). This value is too low as the enthalpy of SS10 crystallization must be superior to this of SS7 (Espinosa-Marzal and Scherer 2008). Thus, this result suggests that SS10 crystallizes through a reaction of hydration (SS7 crystals + $H_20 < - >$ SS10) instead of a direct precipitation from the solution. This interpretation is also supported by the fact that heat flow data do not show any evidence of SS7 dissolution prior to the crystallization of SS10. The second cycle presents similar results except that the crystallization of SS7 and SS10 occur at higher temperatures (+5 °C instead of −3 °C for SS7, and −5 °C instead of −8 °C for SS10). The average enthalpy of SS7 crystallization can be estimated at $\Delta H_m = -22.630$ kJ/mol (with $\Delta n_c = 3.27 \times 10^{-5}$ mol at +5 °C; $Q_{meas} = 0.74$ J) for cycle 2. The calculated value of ΔH_m for the peak attributed to SS10 is very similar to the one calculated for cycle 1 ($\Delta H_m = -20.952$ kJ/mol; with $\Delta n_c = 5.44 \times 10^{-5}$ mol at −5 °C; $Q_{meas} = 1.14$ J), which supports once again, the formation of SS10 via a hydration reaction from SS7 rather than a crystallization from a solution (requiring previously SS7 dissolution). The third cycle shows a different crystallization pattern characterized by the absence of the crystallization's peak of SS7. Therefore, in this case, SS10 crystallizes directly from the solution. The heat flow associated with the SS10 crystallization is much more important than in cycle 1 and 2. The estimated ΔH_m equal to −58.078 kJ/mol ($\Delta n_c = 5.44 \times 10^{-5}$ mol at −5 °C, Q_{meas} from the peak is 3.16 J) is consistent with the value available in Espinosa-Marzal and Scherer (2008) and supports the interpretation of SS10's crystallization from the solution.

SS10 is only observed at negative temperature close to −10 °C using temperature monitoring and DSC (Figs. 5, 7, 8). The ΔT and the heat flow associated with its crystallization are more important than for SS7. As shown by the duration of the formation's peak, SS10 crystallizes almost instantaneously compared to SS7.

Two endothermic reactions are observed corresponding, respectively, to ice melting (reaction 6 only observed with temperature monitoring; Fig. 5) and SS10 dissolution (reaction 7, Figs. 5, 7). Ice melting occurs at temperature close to −2 °C, which is consistent with the phase diagram. The dissolution temperature of SS10 occurs between 18 and 38 °C which is consistent with Hamilton and Hall (2008). The lack of ice crystallization in the DSC results may be due to the undercooling effect. This interpretation is supported by an additional DSC performed on a solution with the same concentration, but between +50 and −40 °C, which showed the crystallization of ice at −25 °C.

The analysis of the different experiments performed in this study show two types of results (cases 1 and 2). In both cases, the experimental conditions were identical (i.e., same salt concentration, same cycles, same analytical facilities—DSC, climatic chamber, type of thermocouple, etc.—research worker), except (1) the nature of the sample holder, (2) the location of the thermocouple, (3) the amount of liquid used and (4) the sample holder preparation. Temperature monitoring was performed within glass bottle, whilst DSC used aluminum cup. It is well known that the substrate composition may influence the crystallization (e.g., Saidov 2012) mainly due to surface roughness properties (e.g., Gunn 1980; Sen and Mukerji 1999; Barrere et al. 2004; Lei et al. 2011). In the temperature monitoring experiments, the thermocouple dips directly into the solution. Then it can act as a favored site of nucleation, which is not the case in DSC because the thermocouple is placed outside of the aluminum pan (i.e., out of the solution); The difference of liquid amount used in both experiments can also play a minor role in acting mainly on the kinetic and the duration of the crystallization/dissolution processes. Finally, the sample holder preparation, and more specifically the drying condition (see "Materials and methods") are very likely to influence strongly the crystallization. Indeed, the results of case 1 were obtained when the sample holder is dried with compressed air, whilst those of the case 2 were obtained when the sample holder is dried by evaporation (either at room T or at +60 °C). Therefore, the conditions of preparation of the sample holder remove or leave some impurities that can explain the difference of crystallization/dissolution sequence observed in cases 1 and 2. This suggests that compressed air drying would be more efficient to remove some impurities that may play a role in crystallization processes occurring in the Na_2SO_4–H_2O system (Fig. 8a). Thus, the presence of impurities in a solution could favor the crystallization of SS10 and ice. Thanks to these two preparation conditions of the sample holder, we managed to distinguish and characterize the thermal signature of both sodium sulfate hydrates (Fig. 8a, b). The temperature monitoring shows that the temperature signature of SS7 is very different to that of SS10. The differences are: the shape, the height and the duration of the crystallization's peak (Table 1). The ΔT related to the crystallization of SS7 reveals a weak and smooth peak with a low intensity occurring over a large period of time. At the opposite, the formation of SS10 is characterized by a narrow peak with an abrupt increase of temperature

occurring over a short period of time. The crystallization of ice has also its own thermal signature, which is characterized by an even more important ΔT than that of SS10 but occurring over a longer period of time.

Conclusion

This study showed that heptahydrate and mirabilite present very different and distinguishable thermal signatures. It enables also to show that mirabilite can crystallize either directly from the cooling of a saturated solution or from a hydration reaction of the heptahydrate. In both cases, the thermal signature is similar, except the peak intensity, which is higher when mirabilite crystallizes directly from the solution. The temperature monitoring allowed us also to observe the dissolution processes. The temperature of dissolution can then be used to identify the nature of the disappearing phase. This work has also highlighted the role of impurities in crystallization process, in particular in the case of ice and mirabilite formation. The DSC results of this study are consistent with previous DSC study (Espinosa-Marzal and Scherer 2008) and they support the temperature monitoring data. They show in addition the existence of undercooling phenomena, especially for ice.

Finally, the temperature monitoring is a simple and economic method to track phase transitions during cooling/heating cycle of a bulk solution. This method will be further used in accelerated aging test performed on porous materials to study the role of the different sodium sulfate hydrates (especially SS7) in salt damaging.

Acknowledgments This work has been financially supported by the Fondation des Sciences du Patrimoine (Patrima) and a PhD grant from the University of Cergy-Pontoise. The LPPI is acknowledged for the access to the DSC facilities. The two anonymous referees are acknowledged for their constructive reviews.

References

Amirthalingam V, Karkhanavala MD, Rao URK (1977) Topotaxic phase change in Na_2SO_4. Acta Crystallogr Sect A Cryst Phys Diffr Theor Gen Crystallogr 33(3):522

Anderson AB (1984) Mechanism for forming hydrogen chloride and sodium sulfate from sulfur trioxide, water, and sodium chloride. J Am Chem Soc 106(21):6262–6265

Barrere F, Snel MM, Van Blitterswijk CA, De Groot K, Layrolle P (2004) Nano-scale study of the nucleation and growth of calcium phosphate coating on titanium implants. Biomaterials 25(14):2901–2910

Bing H, He P, Yang C, Shi Y, Zhao S, Bian X (2007) Impact of sodium sulfate on soil frost heaving in an open system. Appl Clay Sci 35(3):189–193

Correns CW (1949) Growth and dissolution of crystals under linear pressure. Discuss Faraday Soc 5:267–271

De Coppet LC (1901) Sur l'heptahydrate de sulfate de sodium. Bulletin de la Societe Vaudoise des Sciences Naturelles 37:141

Derluyn H, Saidov TA, Espinosa-Marzal RM, Pel L, Scherer GW (2011) Sodium sulfate heptahydrate I: the growth of single crystals. J Cryst Growth 329(1):44–51

Desarnaud J (2009) Mécanisme de croissance et dissolution de cristaux de KCl sous charge: Apport dans la connaissance des mécanismes d'altération des pierres par les sels. Doctoral dissertation Université Paul Cézanne-Aix-Marseille III

Espinosa RM, Franke L, Deckelmann G (2008) Model for the mechanical stress due to the salt crystallization in porous materials. Constr Build Mater 22(7):1350–1367

Espinosa-Marzal RM, Scherer GW (2008) Crystallization of sodium sulfate salts in limestone. Environ Geol 56(3–4):605–621

Flatt RJ (2002) Salt damage in porous materials: how high supersaturations are generated. J Cryst Growth 242(3):435–454

Gans W (1978) Thermodynamic stability of sodium sulfate heptahydrate. Z Phys Chem 111(1):39–46

Genkinger S, Putnis A (2007) Crystallisation of sodium sulfate: supersaturation and metastable phases. Environ Geol 52(2):329–337

Goudie A, Viles HA (1997) Salt weathering hazards. Wiley, Chichester 241

Grossi CM, Esbert RM, del Río LS, Montoto M, Laurenzi-Tabasso M (1997) Acoustic emission monitoring to study sodium sulphate crystallization in monumental porous carbonate stones. Stud Conserv 42(2):115–125

Gunn DJ (1980) Effect of surface roughness on the nucleation and growth of calcium sulphate on metal surfaces. J Cryst Growth 50(2):533–537

Hall C, Hamilton A (2008) The heptahydrate of sodium sulfate: does it have a role in terrestrial and planetary geochemistry? Icarus 198(1):277–279

Hamilton A, Hall C (2008) Sodium sulfate heptahydrate: a synchrotron energy-dispersive diffraction study of an elusive metastable hydrated salt. J Anal At Spectrom 23(6):840–844

Hamilton A, Menzies RI (2010) Raman spectra of mirabilite, $Na_2SO_4{\cdot}10H_2O$ and the rediscovered metastable heptahydrate, $Na_2SO_4{\cdot}7H_2O$. J Raman Spectrosc 41(9):1014–1020

Hamilton A, Hall C, Pel L (2008) Sodium sulfate heptahydrate: direct observation of crystallization in a porous material. J Phys D Appl Phys 41(21):212002

Hartley H, Jones BM, Hutchinson GA (1908) LXXV—The spontaneous crystallisation of sodium sulphate solutions. J Chem Soc Trans 93:825–833

Lei C, Peng Z, Day T, Yan X, Bai X, Yuan C (2011) Experimental observation of surface morphology effect on crystallization fouling in plate heat exchangers. Int Commun Heat Mass Transf 38(1):25–30

Loewel H (1850) Observations sur la sursaturation des dissolutions salines. Ann Chim Phys 29:62–117

Malin MC (1974) Salt weathering on Mars. J Geophys Res 79(26):3888–3894

Marliacy P, Solimando R, Bouroukba M, Schuffenecker L (2000) Thermodynamics of crystallization of sodium sulfate decahydrate in H_2O–NaCl–Na_2SO_4: application to $Na_2SO_4{\cdot}10\ H_2O$-based latent heat storage materials. Thermochim Acta 344(1):85–94

Oswald ID, Hamilton A, Hall C, Marshall WG, Prior TJ, Pulham CR (2008) In situ characterization of elusive salt hydrates: the crystal structures of the heptahydrate and octahydrate of sodium sulfate. J Am Chem Soc 130(52):17795–17800

Pel L, Saidov TA (2013) The thermodynamic and poromechanic crystallization pressure of sodium sulfate heptahydrate: an NMR study. Poromechanics V 782–789. doi:10.1061/9780784412992.094

Pel L, Saidov TA, Espinosa-Marzal RM, Scherer GW (2010) The formation of metastable sodium sulfate heptahydrate in porous materials as studied by NMR. Proceedings of the MEDACHS10 47–54

Rijniers LA, Pel L, Huinink HP, Kopinga K (2005) Salt crystallization as damage mechanism in porous building materials, a nuclear magnetic resonance study. Magn Reson Imaging 23(2):273–276

Rodriguez-Navarro C, Doehne E (1999) Salt weathering: influence of evaporation rate, supersaturation and crystallization pattern. Earth Surf Proc Land 24:191–209

Rodriguez-Navarro C, Doehne E, Sebastian E (2000) How does sodium sulfate crystallize? Implications for the decay and testing of building materials. Cem Concr Res 30(10):1527–1534

Saidov TA (2012) Sodium sulfate heptahydrate in weathering phenomena of porous materials. Doctoral dissertation, Ph. D thesis, Eindhoven University of Technology, The Netherlands

Saidov TA, Espinosa-Marzal RM, Pel L, Scherer GW (2012) Nucleation of sodium sulfate heptahydrate on mineral substrates studied by nuclear magnetic resonance. J Cryst Growth 338(1):166–169

Saidov TA, Shahidzadeh N, Pel L (2013) Crystallization of sodium sulfate on hydrophilic/hydrophobic surfaces during drying: an NMR study. EPL (Europhys Lett) 102(2):28003

Scherer GW (2004) Stress from crystallization of salt. Cem Concr Res 34:1613–1624

Sen S, Mukerji T (1999) A generalized classical nucleation theory for rough interfaces: application in the analysis of homogeneous nucleation in silicate liquids. J Non-Cryst Solids 246(3):229–239

Shahidzadeh-Bonn N, Rafaï S, Bonn D, Wegdam G (2008) Salt crystallization during Evaporation: impact of interfacial properties. Langmuir 24(16):8599–8605

Sperling CHB, Cooke RU (1985) Laboratory simulation of rock weathering by salt crystallization and hydration processes in hot, arid environments. Earth Surf Proc Land 10(6):541–555

Steiger M (2005a) Crystal growth in porous materials—I: the crystallization pressure of large crystals. J Cryst Growth 282(3–4):455–469

Steiger M (2005b) Crystal growth in porous materials—II: influence of crystal size on the crystallization pressure. J Cryst Growth 282(3–4):470–481

Steiger M, Asmussen S (2008) Crystallization of sodium sulfate phases in porous materials: the phase diagram Na_2SO_4–H_2O and the generation of stress. Geochim Cosmochim Acta 72(17):4291–4306

Tsui N, Flatt RJ, Scherer GW (2003) Crystallization damage by sodium sulfate. J Cult Herit 4(2):109–115

Washburn ER, Clem WJ (1938) The transition temperature of sodium sulfate heptahydrate. J Am Chem Soc 60(4):754–757

Winkler EM, Singer PC (1972) Crystallization pressure of salts in stone and concrete. Geol Soc Am Bull 83(11):3509–3514